Journal of Materials Chemistry C

PAPER

View Article Online
View Journal | View Issue

Cite this: J. Mater. Chem. C, 2019, 7, 6359

Synergistic tuning of the optical and electrical performance of AIEgens with a hybridized local and charge-transfer excited state†

Han Zhang,[a] Jiajie Zeng,[a] Wenwen Luo,[a] Haozhong Wu,[a] Cheng Zeng,[a] Kexin Zhang,[a] Weiqiang Feng,[a] Zhiming Wang,*[ab] Zujin Zhao*[a] and Ben Zhong Tang*[ac]

Received 17th March 2019,
Accepted 18th April 2019

DOI: 10.1039/c9tc01453e

rsc.li/materials-c

The reported organic light-emitting diodes (OLEDs) based on hybridized local and charge-transfer (HLCT) state emitters mostly exhibit low photoluminescence quantum yields (PLQYs) in aggregates, failing to achieve optimal device efficiency although they exhibit good exciton utilization efficiencies (EUEs). In this work, by introducing an aggregation-induced emission (AIE) moiety (tetraphenylethene, TPE) and a cyano group (CN) to the HLCT-typed core, phenanthroimidazole (PI), six luminescent compounds with different conjugation patterns at the C2 and N1 substituent positions were obtained, and their excited states were regulated effectively. Based on systematic photophysical analysis, the impacts of molecular conjugation patterns on the regulation of the locally excited (LE) and charge-transfer (CT) components are disclosed, and their AIE characteristics that ensure the high PLQYs of these compounds in aggregates were observed. Exciton conversion channels from triplets to singlets *via* the tuning of excited states were proposed based on theoretical calculations. The non-doped OLED based on *pp*CTPI compounds exhibited excellent performance with a maximum luminance, current efficiency, and external quantum efficiency of up to 31070 cd m^{-2}, 18.46 cd A^{-1}, and 7.16%, respectively, and a very small efficiency roll-off of 4.0% at 1000 cd m^{-2} luminance. The successful design of these HLCT-based AIEgens not only provides more optimization choices for OLED emitters, but also demonstrates that the strategy of reasonably superposing the AIE unit onto HLCT emitters is feasible in materials design.

Introduction

Organic light-emitting diodes (OLEDs) have been extensively developed for practical applications in flat-panel displays and solid-state lighting technologies owing to various superior features such as low energy cost, high brightness, high-quality color, light weight, and flexibility.[1] To achieve high electroluminescence (EL) efficiencies, two main factors of the luminescent materials namely, photoluminescence quantum yields (PLQY) in the solid state and exciton utilization efficiency (EUE), play crucial roles in the working process, which deserve particular attention in materials design. In fact, the EUEs of most traditional fluorescent emitters are theoretically limited to 25% (maximum) from electro-generated singlet excitons according to the spin statistics,[2] but a greater proportion of triplet excitons (75%) failed to generate photons and are lost through non-radiative decay because of spin-forbidden transitions from the triplet to singlet state. Therefore, harvesting triplet excitons for light emission has been recognized as an effective strategy to increase EL efficiencies in OLEDs.

Currently, thermally activated delayed fluorescence (TADF),[3] triplet–triplet annihilation (TTA)[4] and hybridized local and charge-transfer (HLCT) state[5] mechanisms were developed to solve the problem of triplet exciton utilization in pure organic

[a] SCUT-HKUST Joint Research Institute, Guangzhou International Campus, Center for Aggregation-Induced Emission, State Key Laboratory of Luminescent Materials and Devices, South China University of Technology, Guangzhou 510640, China. E-mail: wangzhiming@scut.edu.cn, mszjzhao@scut.edu.cn
[b] School of Petrochemical Engineering, Shenyang University of Technology, Liaoyang 111003, China
[c] Department of Chemistry, Hong Kong Branch of Chinese National Engineering Research Center for Tissue Restoration and Reconstruction, The Hong Kong University of Science and Technology, Clear Water Bay, Kowloon, Hong Kong, China. E-mail: tangbenz@ust.hk

† Electronic supplementary information (ESI) available: Experimental details, X-ray crystallography, device fabrication, TGA curves and DSC spectra, PL spectra in THF, additional AIE curves, time-resolved fluorescence decay curves in THF solutions and neat films, detailed theoretical calculations data, mechanochromism properties measurement and ^{1}H and ^{13}C NMR spectra. CCDC 1903655. For ESI and crystallographic data in CIF or other electronic format see DOI: 10.1039/c9tc01453e

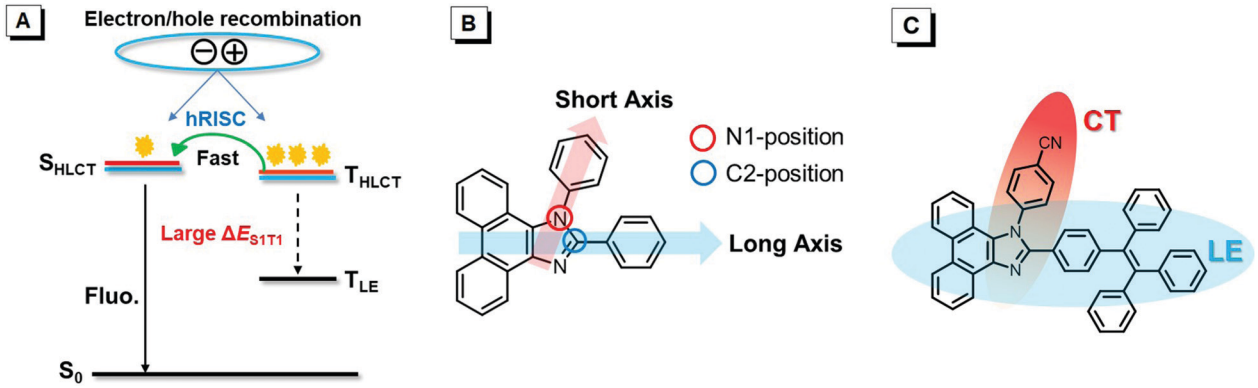

Fig. 1 (A) Typical energy level characteristics of an HLCT emitter with a "hot exciton" channel; (B) the long-short axis design based on phenanthroimidazole in this work. (C) Construction of the LE state and the CT state in the PI derivative (taking *pp*CTPI as an example).

emitters. Actually, considerable successes have been achieved based on these mechanisms, leading to the greatly boosted EL efficiencies of noble-metal free organic emitters. Among them, the HLCT mechanism has drawn increasing attention in recent years because it is conducive to both PLQY and EUE.[6] In HLCT emitters (Fig. 1A), the dominant locally excited (LE) component in the hybridized state at low-lying S_1 is liable to fluoresce intensely due to a large overlap between hole and electron wave functions and generate a large singlet–triplet energy splitting between S_1 and T_1 ($\Delta E_{S_1T_1}$); whereas at high-lying levels, the charge-transfer (CT) component in the hybridized state leads to the activation of the "hot exciton" channels with a negligible $\Delta E_{S_mT_n}$ ($m \geq 1$, $n \geq 2$), enabling the reverse intersystem crossing (RISC) process and thus increasing the EUE.[6d] The EUEs of many reported HLCT emitters are close to 100%, but their PLQYs are not high enough in neat films in practice due to the aggregation-caused quenching (ACQ) phenomenon, which undermines their EL performance.[5d,6c] In addition, seeking molecular design strategies and excited state modulation principles for HLCT emitters is still a challenging task.

Recently, aggregation-induced emission (AIE) offers a high possibility of solving the ACQ problem of most traditional chromophores,[7] and the luminogens with AIE characteristics (AIEgens)[8] can fluoresce intensively when they are fabricated into neat films, which are considered as ideal light-emitting materials for non-doped OLEDs.[9] Hence, it is a promising strategy to achieve a win–win situation by combining the HLCT process with AIE nature.[10] Herein, we chose a typical HLCT unit, phenanthroimidazole (PI), to function as an emissive core in the molecular design (Fig. 1B and C),[11] and a star AIE molecule, TPE, was introduced into the C2-position of imidazole ring in PI (defined as the long axis in molecular structure) with different patterns (*para*- and *meta*-linkages). Thus, we can tune the LE component in hybridized excited states and luminescence behaviors in the aggregated states *via* different conjugated degrees. At the N1-position (defined as the short axis in molecular structure), a benzonitrile with a cyano group (CN) at the *meta*- or *para*-pattern was inserted to tune the CT component in the HLCT state. Then, six AIEgens, *p*TPI,[12a] *mp*CTPI, *pp*CTPI, *m*TPI, *mm*CTPI and *pm*CTPI, were synthesized and

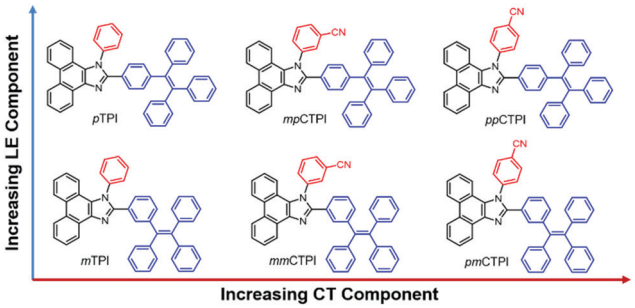

Fig. 2 Chemical structures of the six PI derivatives.

characterized (Fig. 2). The substituent effects on their photophysical and electrochemical properties of the six compounds were systematically investigated. They showed prominent AIE characteristics and high PLQYs in aggregates. Their EUEs can be enhanced by tuning the excited state to promote exciton conversion channels based on theoretical calculations, which was confirmed in subsequent EL performances. The non-doped OLED using *pp*CTPI as an emitter exhibited the best EL performance with excellent external quantum efficiency (7.16%, EQE) and EUE (>48%), and its maximum luminance, current efficiency, and power efficiency (L, η_c, and η_p) reached 31 070 cd m^{-2}, 18.46 cd A^{-1} and 16.32 lm W^{-1}, respectively. In addition, the ultra-low roll-off of 4.0% at 1000 cd m^{-2} luminance was observed. These results demonstrated a feasible strategy of tuning excited state distributions by reasonably combining HLCT materials with AIE nature for the development of high-efficiency emitters for OLEDs.

Results and discussion

Synthesis and crystal structure

Phenanthrenequinone, the corresponding aromatic amines, aromatic aldehydes and ammonium acetate were chosen to obtain the target compounds *via* a one-pot reaction in good yields. The detailed synthetic routes, preparation methods and characterization data of these final products are described in

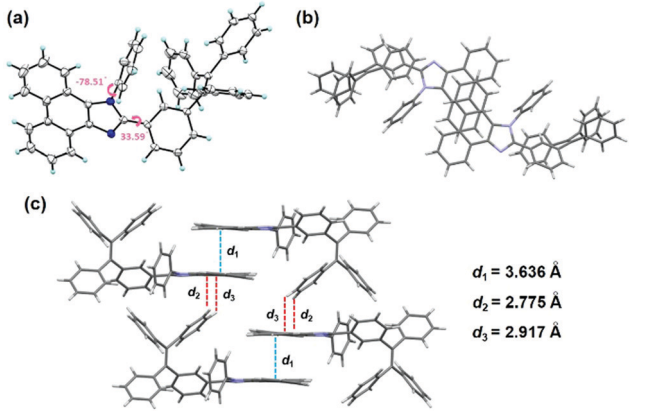

Fig. 3 (a) ORTEP drawing of the crystal structure (CCDC 1903655) of *m*TPI and (b and c) packing pattern of *m*TPI in crystals.†

the ESI† (Fig. S1). The single crystals of *m*TPI were grown from the ethanol and dichloromethane mixture by slow solvent diffusion and evaporation. As depicted in Fig. 3, a twisted conformation with a large dihedral angle of 78.51° and a planar conformation with a small dihedral angle of 33.59° were observed at the N1-position and C2-position of *m*TPI, respectively. The molecular packing of *m*TPI shows an antiparallel arrangement, in which TPE and PI units form a head-to-tail stacking. As a result, the twisted TPE unit can interrupt the π–π stacking interactions among PI units with an interplane distance of 3.636 Å. The distances of 2.775 Å and 2.917 Å between the hydrogen atoms of the TPE phenyl rings and the π-electrons of PI indicate that C–H···π hydrogen-bond interactions existed in the crystals, which can restrict and lock the molecular rotations of TPE and lead to the reduction of the non-radiative energy loss *via* rotational relaxation.[12b]

Thermal properties

The thermal properties of the six compounds were examined using thermogravimetric analysis (TGA) and differential scanning calorimetry (DSC) methods under N_2 atmosphere. As shown in Fig. S2 (ESI†) and Table 1, all the compounds exhibited high thermal decomposition temperatures (T_d, corresponding to 5% weight loss) in the range of 389–443 °C. Moreover, the four cyano-containing compounds had better thermal stabilities, similar to our previous findings.[11a] DSC measurements were carried out from 30 °C to 360 °C, and the three TPE *meta*-linked compounds, *m*TPI, *mm*CTPI and *pm*CTPI, revealed distinct glass transition temperatures (T_g) of 114 °C, 126 °C and 128 °C, respectively. No evident T_g peaks could be detected in their counterparts, but crystallization temperatures (T_c) of 202 °C for *p*TPI and 210 °C for *mp*CTPI were observed. These results indicated the good thermal and morphological stabilities of the six compounds, which would have positive effects on the performance of their OLED devices.

Photophysical properties

Fig. 4A shows the ultraviolet-visible (UV-vis) absorption spectra of the compounds in tetrahydrofuran (THF, [c] = 1×10^{-5} M). The sharp absorptions at 260 nm in all compounds were considered as the typical π-electron response of the phenanthrene derivative.[11b] The long-wavelength absorption bands at 300–370 nm might be attributed to the π–π* transitions at the long-axis direction.[11b,13] Red-shifted and enhanced absorption bands were found in the TPE *para*-linked compounds because of their more effective conjugation than TPE *meta*-linked ones. Interestingly, there was a negligible change in the absorption spectra before and after the cyano group introduction, which indicated that the ICT effect along the N1-substitution direction had little influence on the absorption process and optical bandgaps of the compounds.

The photoluminescence (PL) spectra of these compounds in dilute THF solutions (10^{-5} M) and neat films were displayed in Fig. S3 (ESI†) and Fig. 4B. In THF solutions, three TPE *para*-linked compounds exhibited blue emissions ranging from 409 to 487 nm with hyperfine vibrational structures in their PL spectra, indicating that LE components were dominant in their HLCT states according to the previous reports about PI-based derivatives.[5a,12a] When the linkage of the TPE unit was changed into the *meta*-linked form, their conjugation degree in the long-axis direction decreased, resulting in bluer emissions and less LE components. However, their hyperfine vibrational structure vanished gradually after cyano group insertion, and the emission was red-shifted at the same time, implying increased CT proportion in the short-axis direction. In the vacuum-deposited neat films, *p*TPI, *mp*CTPI and *pp*CTPI showed broad PL peaks at 493, 503 and 501 nm, respectively, and the other three emitted sky-blue PL ranging from 491 to 493 nm. In comparison with those in

Table 1 Photophysical and thermal properties of the compounds[a]

	λ_{abs} (nm)	λ_{em} (nm)			Φ_F (%)			α_{AIE}	τ (ns) [k_r (ns^{-1}), k_{nr} (ns^{-1})]		T_g/T_d (°C)
		Soln	Aggr	Film	Soln	Aggr	Film		Soln	Film	
*p*TPI	365	432, 465	483	493	0.3	69.4	88.5	231.3	0.73 (0.004, 1.366)	2.63 (0.337, 0.044)	nd/389
*mp*CTPI	361	433, 461	485	503	0.5	64.2	67.2	128.4	0.84 (0.006, 1.185)	2.37 (0.284, 0.138)	nd/443
*pp*CTPI	361	433, 460	475	501	0.5	61.2	59.5	122.4	1.06 (0.005, 0.939)	2.85 (0.209, 0.142)	nd/415
*m*TPI	362	389, 410	465	491	0.5	39.4	47.6	78.8	1.03 (0.005, 0.966)	4.19 (0.114, 0.125)	114/402
*mm*CTPI	359	389, 412	464	493	0.6	33.5	23.8	55.8	1.94 (0.003, 0.512)	3.97 (0.060, 0.192)	126/408
*pm*CTPI	359	423	467	492	1.2	31.3	20.5	26.1	1.14 (0.011, 0.867)	4.26 (0.048, 0.187)	128/414

[a] soln = THF solution (10^{-5} M); aggr = nanoaggregate formed in H_2O/THF mixture with a f_w of 90%; film = vacuum-deposited neat film; Φ_F = absolute PL quantum yield determined by a calibrated integrating sphere; α_{AIE} = value of the AIE effect, calculated by Φ_F(aggr)/Φ_F(soln); τ = PL lifetimes measured at room temperature in air; k_r = radiative decay rate ($k_r = \Phi_F/\tau$); k_{nr} = nonradiative decay rate ($k_{nr} = (1 - \Phi_F/\tau)$); nd = not detectable.

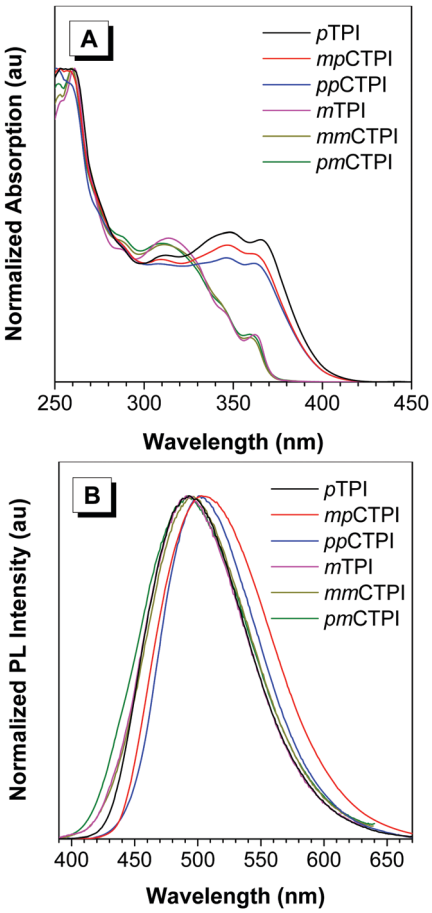

Fig. 4 (A) Absorption spectra in THF solutions (10^{-5} M) and (B) PL spectra of neat films of the compounds.

solutions, the emission peaks in the films were considerably redshifted. This is because the molecular packing in the films can decrease the degree of twisting of the TPE unit, thus prolonging the conjugation length and giving rise to a large redshift. All compounds were weakly fluorescent with low absolute PL quantum yields (Φ_F) of 0.3–1.2% in THF solutions, but emitted intensely in neat films, demonstrating notable AIE nature. The Φ_Fs of TPE *para*-linked compounds in neat films were higher than those of their counterparts because of the enlarged degree of the effective π-conjugation at the long-axis, and *p*TPI had the highest value of 88.5%. Upon the addition of the cyano group, the Φ_Fs of the emitters decreased, indicating that the increment of CT-component had a negative effect on their luminescence efficiencies. It was worth noting that the six compounds exhibited mechanochromism properties.[12a] The PL emissions of neat films were closer to the ones from the ground states (see ESI†), indicating the formation of amorphous states in the vacuum deposition films. Their absolute Φ_Fs in different states were listed in Table 1. Solvatochromic effects on PL was used to examine complex HLCT changes in the composition.[5a,14] However, the emissions in some high-polar solvents were too weak to detect accurately because of their faint fluorescence caused by their AIE nature. Therefore, the tuning processes of LE and CT distribution and proportion were confirmed by theoretical calculations instead.

To investigate their AIE characteristics, water, a poor solvent of the compounds, was added into their THF solutions in different proportions (Fig. 5 and Fig. S4, ESI†). The emissions of the six compounds were very weak at a low water fraction (f_w) but became stronger as the f_w increased. Consequently, their Φ_Fs exhibited dozen and even hundred-fold enhancement under aqueous conditions. The greatly enhanced PL efficiencies should be attributed to the restriction of rotational motions by the spatial constraint in the aggregated state and thus the suppression of nonradiative decay of the excited state.[15] To further understand the relevant photophysical process, the transient fluorescence spectra were measured (Fig. S5, ESI†). As listed in Table 1, all the compounds showed longer fluorescence lifetimes in neat films than in THF solutions. Their non-radiative decay rates (k_{nr}) decreased greatly from solutions to films, which enabled them to emit more efficiently in aggregates with significant improvement in PLQYs. The compounds showed a single-index decay of lifetime without a delayed component, which confirmed that there were no TADF or TTA mechanisms in the luminescence process of these compounds.[16]

Electrochemical properties and theoretical calculations

The CV measurements were conducted in CH_2Cl_2 for the oxidation potentials and DMF for the reduction potentials using 0.1 M tetra-*n*-butylammonium-hexafluoro-phosphate (*n*-Bu_4NPF_6) as the electrolyte. The HOMO and LUMO energy levels were determined using ferrocene (Fc) as the reference (4.8 eV) and were calibrated with respect to $E_{1/2}$ (Fc/Fc^+) in every measurement.[17] Their cyclic voltammograms are given in Fig. S6 (ESI†) and the corresponding data are summarized in Table 2. The HOMO energy levels of *p*TPI, *mp*CTPI, *pp*CTPI, *m*TPI, *mm*CTPI and *pm*CTPI were calculated to be −5.49, −5.54, −5.55, −5.56, −5.63, and −5.64 eV, respectively, which were similar to those of the reported PI-based derivatives.[11] The LUMO energy levels of *p*TPI and *m*TPI were estimated to be −2.44 eV and −2.34 eV and were probably populated on the TPE (as an acceptor compared to PI). The other four compounds with cyano groups had lower LUMO energy levels of −2.53, −2.54, −2.51, and −2.50 eV, indicating that the distribution of LUMOs had changed. For further comparison, the electrical bandgaps (E_g^e) of the compounds became narrower after the cyano group insertion, quite different from their optical bandgaps (E_g^o) discussed in the absorption spectra. Such measurement results indicated that there might be character of separation of the electrical and optical energy gaps in cyano-containing compounds, which could be beneficial in constructing a lower injection/transport barrier in wide-bandgap luminescent materials.[18]

To further understand the different energy gaps obtained from absorption spectra and CV measurements, density functional theory (DFT) calculations were carried out at a level of M0-62X/6-31G(d,p), employing the Gaussian 09 package. The geometries, molecular orbitals (MOs) and calculated energy levels are shown in Fig. 6 and Fig. S7 (ESI†). The HOMOs of the compounds were mainly located on the PI unit and TPE

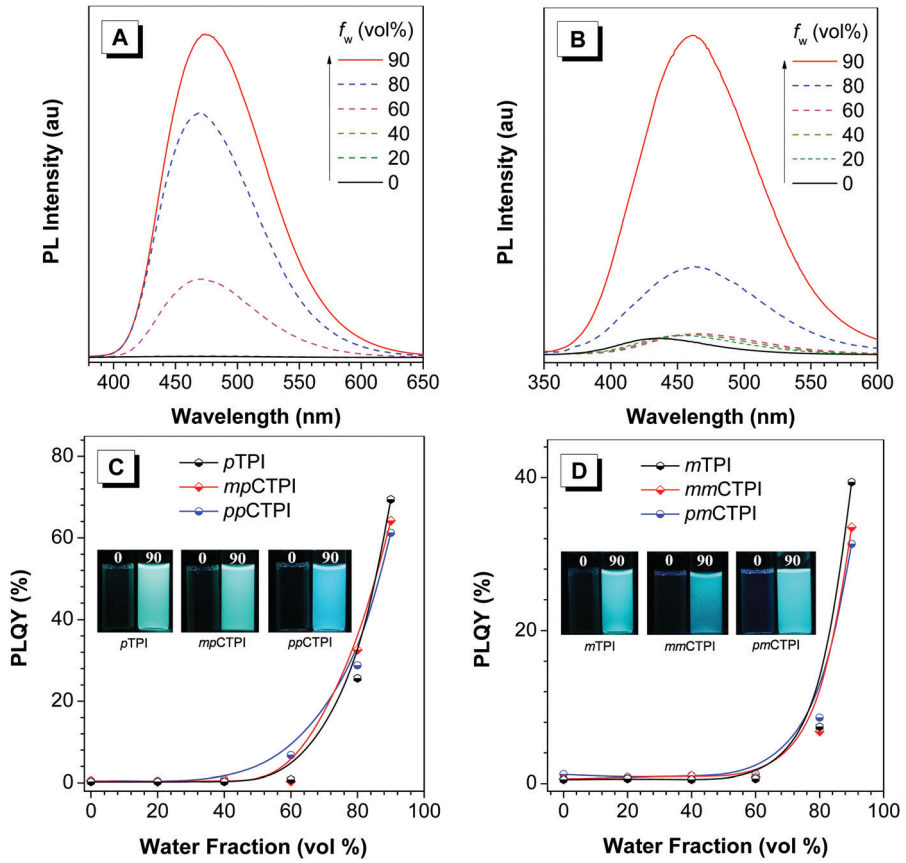

Fig. 5 PL spectra of (A) *pp*CTPI, (B) *pm*CTPI in THF/water mixtures (10^{-5} M) with different water fractions (f_w); (C and D) PLQY *versus* f_w curves; inset: photos of the compounds in THF/water mixtures (f_w = 0 and 90%), taken under 365 nm excitation.

Table 2 Electrochemical data of the compounds[a]

	E^{ox}_{onset} (V)	E^{red}_{onset} (V)	HOMO (eV)	LUMO (eV)	E^{e}_{g} (eV)	E^{o}_{g} (eV)
*p*TPI	0.92	−2.29	−5.49	−2.44	3.05	3.13
*mp*CTPI	0.97	−2.20	−5.54	−2.53	3.01	3.14
*pp*CTPI	0.97	−2.19	−5.55	−2.54	3.01	3.14
*m*TPI	0.99	−2.38	−5.56	−2.34	3.22	3.34
*mm*CTPI	1.06	−2.22	−5.63	−2.51	3.12	3.34
*pm*CTPI	1.07	−2.24	−5.64	−2.50	3.13	3.34

[a] E^{ox}_{onset}: onset oxidation potential; E^{red}_{onset}: onset reduction potential; E^{e}_{g} = LUMO–HOMO; E^{o}_{g} = 1240/λ, λ gained from the absorption spectra.

moiety in the long-axis direction, and small decrements were observed in their calculated HOMO values after the cyano group was inserted. The LUMOs of both *m*TPI and *p*TPI were mostly populated on the TPE acceptor, which well agreed with the analysis above. After inserting the cyano group, the distribution of the LUMOs was transferred into the N1-imidazole position owing to their enhanced electron-withdrawing abilities,[11c] and these lower LUMO values of cyano-containing compounds agreed with the results of the electrochemical measurements. Interestingly, the LUMO+1 levels of the compounds with a cyano group were located mostly in the TPE unit, similar to their respective matrix situations (LUMOs in *m*TPI and *p*TPI). Their calculated energy gaps from the HOMO to the LUMO+1 were 5.63 eV for *mp*CTPI, 5.71 eV for *pp*CTPI, 5.94 eV for *mm*CTPI, and 5.97 eV for *pm*CTPI, and these values were close to the energy gaps from the HOMO to the LUMO in *p*TPI and *m*TPI (5.60 eV and 5.91 eV, respectively). Exactly, these results were consistent with the optical bandgaps obtained from the absorption spectra, confirming the hypothesized separation of the electrical and optical energy gaps. In fact, the transitions from the HOMO to the LUMO in non-cyano-containing compounds and from the HOMO to the LUMO+1 in cyano-containing compounds were allowed because of their effective overlaps in the MOs. However, the transitions from the HOMO to the LUMO in the latter were nearly forbidden in the photo-absorption process, owing to the complete separation characters, wherein the large twisting dihedral angles between the N1-phenyl and PI plane (78° for *p*TPI, 77° for *mp*CTPI, 75° for *pp*CTPI, 80° for *m*TPI, 77° for *mm*CTPI and 76° for *pm*CTPI) contributed considerably to the separation of the MOs.[19]

Excited state properties

In order to examine the excited state properties of the compounds, natural transition orbitals (NTOs) for the $S_0 \rightarrow S_n$ and T_n (n = 1–8) transitions were performed using time-dependent density functional theory (TD-DFT) (Tables S2–S7 and Fig. S8, ESI†).[20] As shown in Fig. 7, for the $S_0 \rightarrow S_1$ transition in *p*TPI, the "hole" and "particle" were mostly located on the imidazole ring and TPE moiety. This distribution was assigned to the LE

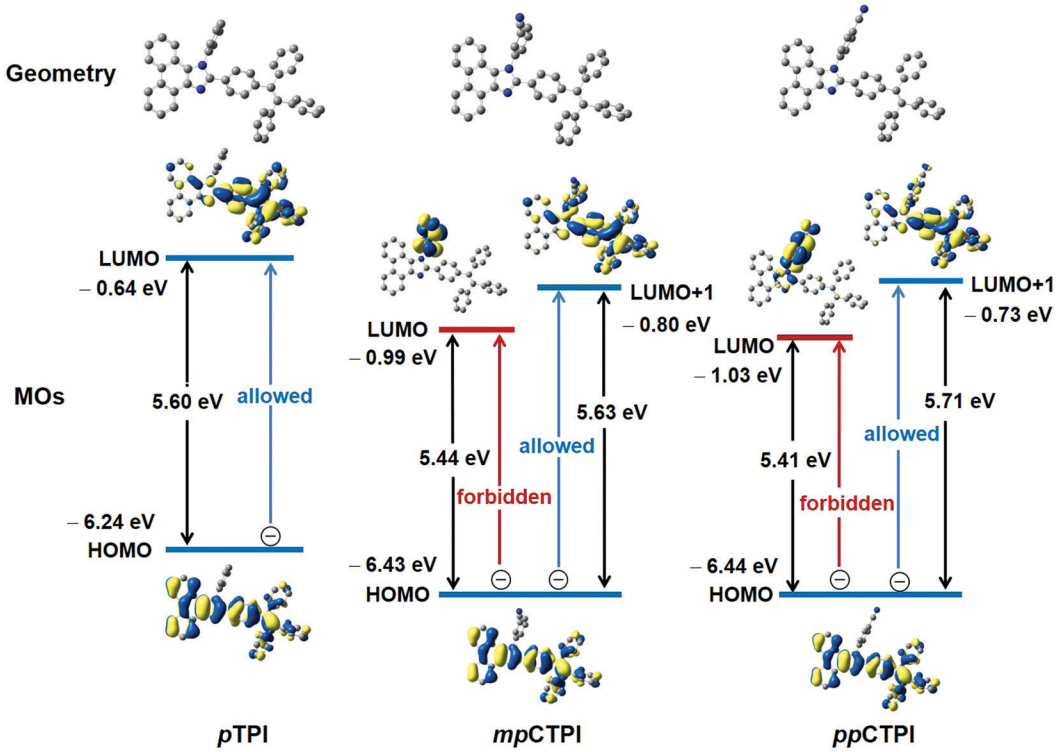

Fig. 6 Relevant molecular orbital amplitude plots, energy levels and possible transition sketch maps of TPE *para*-linked compounds.

transition, and the large overlap of the NTO in TPE implied that the compounds would have a high fluorescence efficiency and AIE characteristics.[12a] The homologous LE character of the PI moiety was also observed in the $S_0 \rightarrow S_2$ transition. Along with the introduction of a cyano group into N1-phenyl, the ICT process was activated and the distribution of NTOs became more complicated. In *mp*CTPI, the $S_0 \rightarrow S_1$ transition exhibited nearly the same LE configuration with *p*TPI, but the distinct CT transition with the "hole" in PI and the "particle" in N_1–CN-phenyl could be found in the $S_0 \rightarrow S_2$ transition, implying that the high-energy CT state was constructed in its excited states, as we expected. When the cyano group was linked at the *para*-position, the increased electron-withdrawing ability in the short-axis direction generated a larger CT component in *pp*CTPI, which could contribute to the $S_0 \rightarrow S_1$ transition. The "hole" and "particle" NTOs for S_1 and S_2, taking on partial

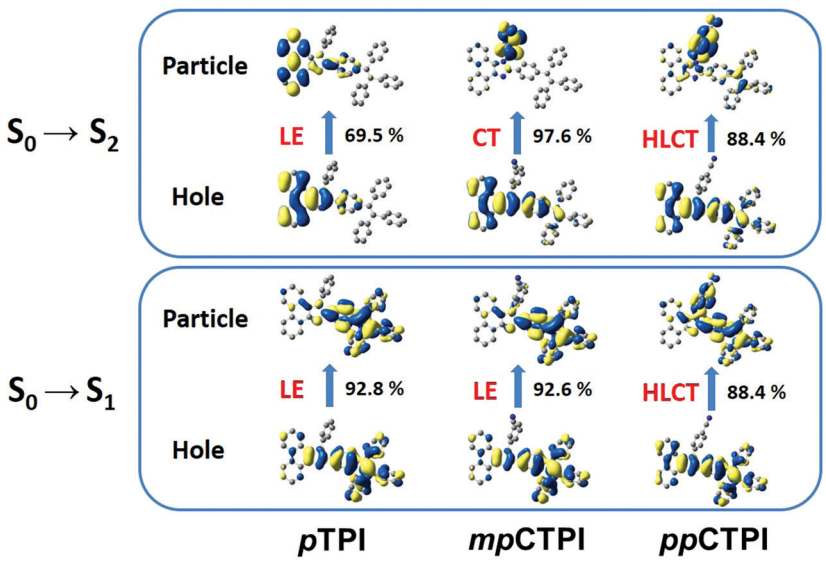

Fig. 7 Natural transition orbitals and properties of $S_0 \rightarrow S_1$ and $S_0 \rightarrow S_2$ for *p*TPI, *mp*CTPI and *pp*CTPI, calculated by the M06-2X hybrid functional at the basis set level of 6-31G(d,p).

separation and partial overlap, were considered as typical HLCT states.[5d,6b] A similar situation arose in the TPE *meta*-linked compounds (Fig. S9, ESI†), wherein, *mm*CTPI and *pm*CTPI contained a better mixed LE/CT component than *m*TPI. However, higher CT components in *mm*CTPI and *pm*CTPI were observed because of the lower conjugation degree caused by the TPE *meta*-linked pattern. Importantly, the oscillator strength of $S_0 \rightarrow S_1$ ($f_{S_0\text{–}S_1}$) that was considered to be related to the PLQYs of the emitters was reduced upon the addition of the cyano group, with values of 0.9570 for *p*TPI, 0.9490 for *mp*CTPI and 0.8102 for *pp*CTPI (in contrast, 0.3324 for *m*TPI, 0.2711 for *mm*CTPI and 0.0642 for *pm*CTPI). These obvious decreases in the oscillator strength were in good agreement with the PLQYs in the experimental measurements (Table 1).

Compared with the common materials based on D–A or the D–π–A system, this two-dimensional vertical conformation–based long-short axis had a larger regulation space for the CT proportion. The lowest luminous state remained LE-like in character when the cyano group was inserted into the N1-position at the short axis, and there was only the increment in the CT-component proportion in every excited-state energy level. This feature had been mentioned in our previous reports: at the long axis of the emitter, the LE-dominated emissive state based on large π-conjugated structure needed to be constructed; and in the vertical direction, a short axis with evident CT character was built with large steric hindrance (the conjugation degree was not too large, or this short axis would become the emission axis).[6c,11] Hence, tunable CT-components could be incorporated into the LE emissive state to form the HLCT state. Combining AIE characteristics further, the PLQYs in the solid-state would be enhanced synchronously.

Why was the CT state required in the process of luminescence? In fact, the CT component does have a negative effect on PLQYs, but it is liable to increase EUEs *via* RISC channels.[3a,5a,6c] For the "hot exciton" based on the HLCT mechanism, the complete conversion of excitons from triplet to singlet states must meet three requirements in the EL process: small $\Delta E_{S_mT_n}$ ($m \geq 1$, $n \geq 2$), CT component with a weak exciton binding energy and an obstacle for exciton relaxation from T_n to T_1.[6d,21] The CT-type exciton usually has a lower binding energy, and its generation is easier than the LE-type exciton after carrier injection and recombination, different from the PL process. In other words, the formation of T_4 (CT-dominant) for *pp*CTPI was easier than T_1 (LE-dominant) in OLEDs, and excitons might be converted into singlet states from T_4 if there was a fast conversion channel. So, intrinsically, the appropriate proportion of the CT component was very important to enhance the EUEs. By comparing all the detailed results of the excited states (Tables S8–S13, ESI†), some valuable tendencies were observed. In *p*TPI and *m*TPI, every excitation in the eight NTOs for triplet states mainly exhibited LE character, as a result of the ineffective RISC path to S_1 or S_2 ($T_{LE} \rightarrow S_{LE}$). For the high-lying S_2 and T_8 in *mp*CTPI, we found that their ΔE_{ST} was very close to the value of 0.05 eV, and both showed obvious CT character from the NTOs, so the triplet excitons might be converted to singlet excitons *via* the RISC channel ($T_{HLCT} \rightarrow S_{CT}$). As the CT component became larger in the other three cyano-containing compounds, the NTOs of both S_1 and S_2 took on HLCT character, and more CT channels, such

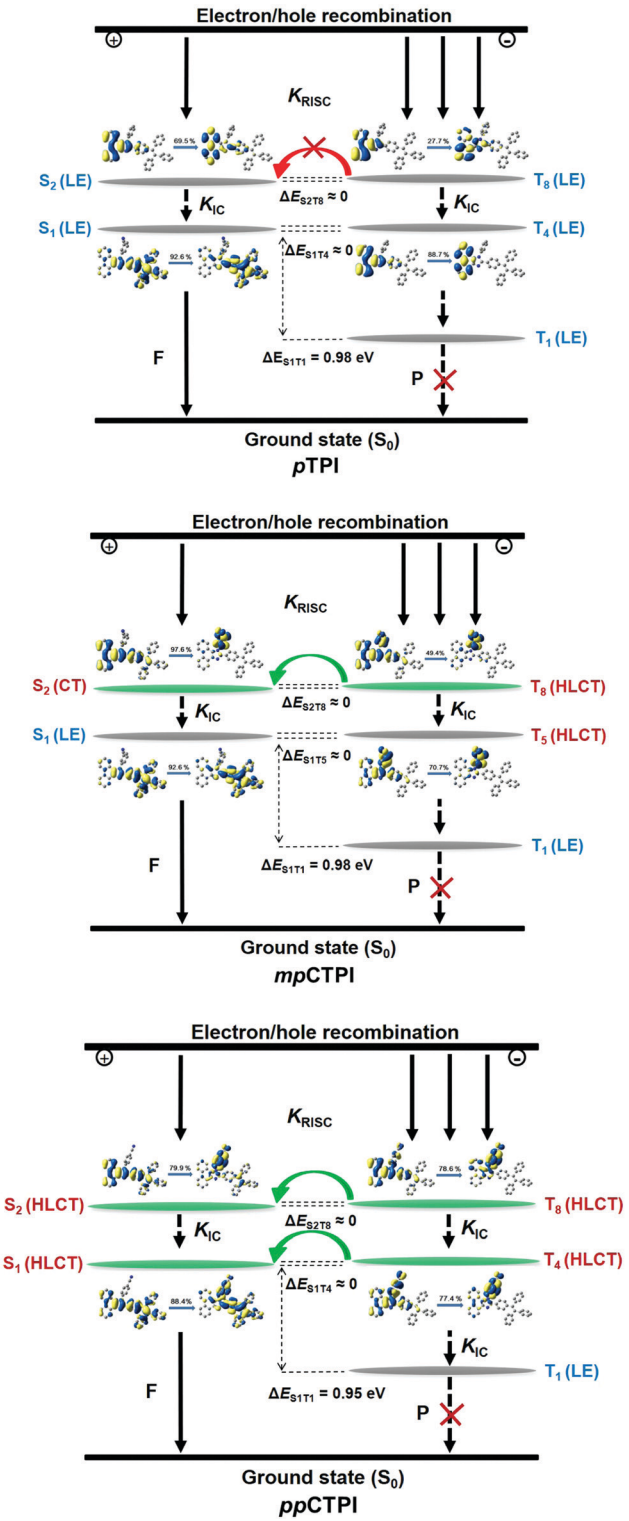

Fig. 8 Probable "hot exciton" mechanism caused by the HLCT states for TPE *para*-linked compounds. S: singlet state; T: triplet state; LE: local excited-state; CT: charge-transfer state; ΔE_{ST}: singlet–triplet energy splitting; K_{IC}: internal conversion rate; K_{RISC}: reverse intersystem crossing rate.

as S_1 and T_4 ($T_{HLCT} \rightarrow S_{HLCT}$) as well as S_2 and T_8 ($T_{HLCT} \rightarrow S_{HLCT}$), could be found that generated more singlet excitons through more effective exciton up-conversion channels, as shown in Fig. 8 and Fig. S10 (ESI†). It was worth noting that the existence of several lower triplets (like T_2 and T_3 in *pp*CTPI) were unfavorable to the RISC process and thus might cause losses when harvesting triplet excitons.

EL performances

If the discussions above were correct, a gradual increment in the EUEs could be expected in the OLED performance. To evaluate their EL properties, we fabricated non-doped OLEDs with a device configuration of ITO/HATCN (5 nm)/TAPC (40 nm)/TCTA (5 nm)/emitters (20 nm)/TmPyPB (40 nm)/LiF (1 nm)/Al (120 nm) (emitters = *p*TPI, device I; *mp*CTPI, device II; *pp*CTPI, device III; *m*TPI, device IV; *mm*CTPI, device V; *pm*CTPI, device VI), where HATCN (dipyrazino[2,3-*f*:2′,3′-*h*]quinoxaline-2,3,6,7,10,11-hexacarbo-nitrile) and LiF served as the hole- and electro-injection layers, respectively; TAPC (di-(4-(*N*,*N*-ditolyl-amino)-phenyl)cyclohexane) and TmPyPB (1,3,5-tri(*m*-pyridin-3-ylphenyl)benzene) worked as the hole- and electron-transporting layers, respectively; 4,4′,4″-tris(carbazol-9-yl)-triphenylamine (TCTA) was used as the exciton blocking layer; and ITO (indium tin oxide) and Al were used as the anode and electrode, respectively. The schematic energy level diagrams of the devices, the EL spectra at 10 mA cm^{-2}, the current density–voltage–luminance (*J*–*V*–*L*) characteristics, the EQE *versus* luminance curves and the current efficiency *versus* luminance curves of the non-doped OLEDs are displayed in Fig. 9. The key data of the device performances are summarized in Table 3, in which the EUE was calculated by eqn (1):

$$\eta_{EL} = \eta_{rec} \times \eta_s \times \eta_{PL} \times \eta_{out} \quad (1)$$

where η_{EL} is the EQE, η_{rec} is the electron–hole recombination proportion (assumed to be 100%), η_s is the EUE, η_{PL} is the PLQY of neat film, and η_{out} is the light out-coupling efficiency (usually estimated from 20% to 30% and calculated using 25% here).[22]

As shown in the EL spectra, the devices based on TPE *para*- and *meta*-linked compounds exhibited bluish green and sky-blue emissions, respectively, and their EL peaks were close to their PL peaks of neat films. All the devices exhibited low turn-on voltages (V_{on}) of under 3.5 eV, owing to the bipolar properties from the PI unit.[23] Among them, the TPE *para*-linked compounds displayed lower V_{on} than *meta*-linked ones because of more balanced carrier transport stemming from their larger molecular conjugation.[24] Enjoying the higher PLQYs, the former exhibited better EL performances than the latter. The EQE_{max} of *p*TPI, *mp*CTPI and *pp*CTPI were 6.32%, 6.71%, and 7.16%, respectively, much higher than those of *m*TPI (3.98%), *mm*CTPI (2.27%) and *pm*CTPI (2.48%). In addition, the cyano group had a very positive effect on increasing the EUE. For *p*TPI and *m*TPI, the EUE values were calculated to be 28% and 33.4%, respectively, which had slightly exceeded the theoretical limit of the spin statistics of fluorescent emitters. For the cyano-containing compounds, the EUE increased noticeably because

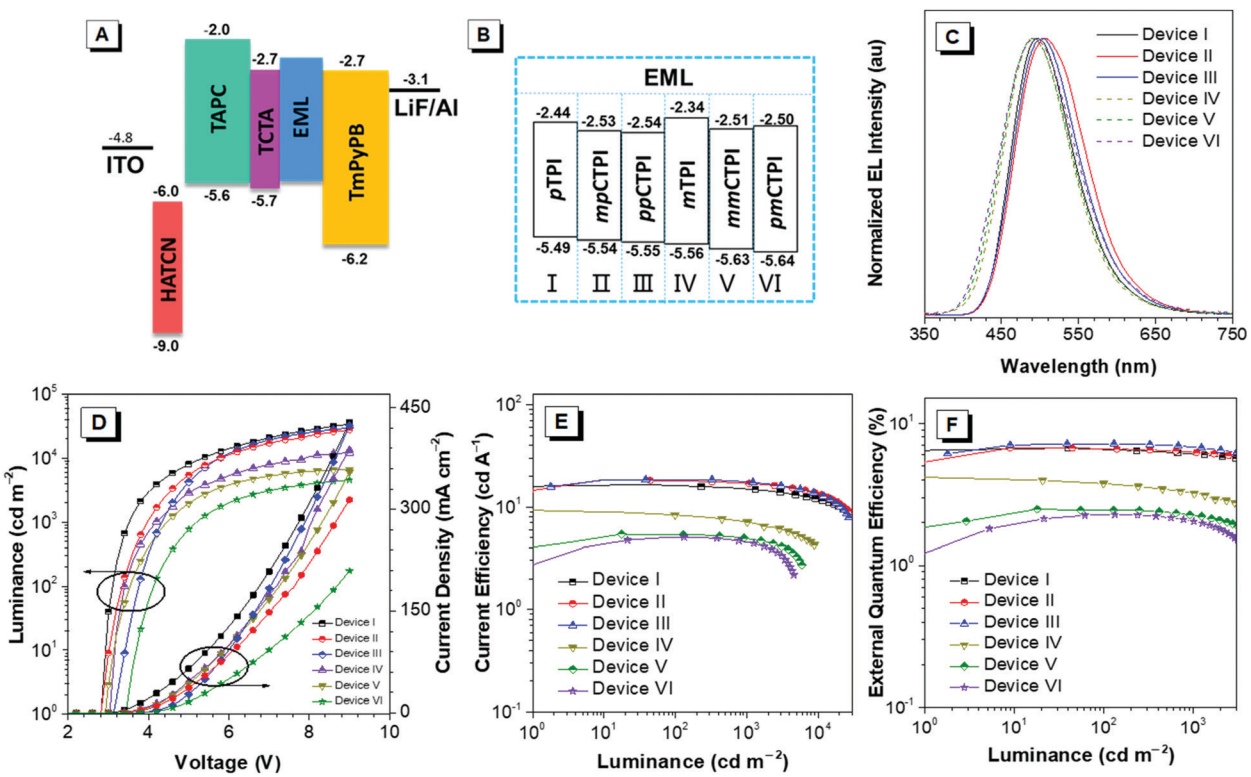

Fig. 9 (A and B) Energy level diagrams; (C) EL spectra at 10 mA cm^{-2}; (D) current density–voltage–luminance (*J*–*V*–*L*) characteristics; (E) current efficiency *versus* luminance curves; and (F) EQE *versus* luminance curves of the non-doped OLEDs based on the six AIEgens.

Table 3 EL performances of the OLEDs based on the compounds

Compounds	Device	λ_{EL} (nm)	V_{on}[a] (V)	L[b] (cd m^{-2})	η_c[b] (cd A^{-1})	η_p[b] (lm W^{-1})	CIE[c] (x, y)	EUE (%)	EQE$_{max}$[b] (%)	EQE$_{1000}$ (%)	RO (%)
*p*TPI	I	494	2.9	40 290	16.52	15.55	(0.226, 0.423)	28.6	6.32	6.07	4.0
*mp*CTPI	II	506	2.9	36 030	18.27	19.12	(0.243, 0.447)	39.9	6.71	6.26	6.7
*pp*CTPI	III	503	3.1	31 070	18.46	16.32	(0.211, 0.402)	48.1	7.16	6.83	4.6
*m*TPI	IV	492	3.1	12 310	8.87	8.70	(0.201, 0.339)	33.4	3.98	3.23	18.8
*mm*TPI	V	493	3.5	5386	5.07	3.93	(0.213, 0.345)	38.2	2.27	2.14	5.7
*pm*TPI	VI	489	2.9	6748	5.44	5.34	(0.195, 0.342)	48.4	2.48	2.04	17.7

[a] V_{on} is the turn-on voltage at 1 cd m^{-2}. [b] The luminescence (L), current efficiency (η_c), power efficiency (η_p) are the maximum values of the devices. [c] CIE coordinates at 10 mA cm^{-2}.

of larger CT component in the HLCT states. When the cyano group was linked in the *para* position, the EUE reached excellent values of 48.1% for *pp*CTPI and 48.4% for *pm*CTPI. The improvement in the EUEs was consistent with the above analysis of more exciton conversion channels. Furthermore, taking advantage of the AIE property, low-efficiency roll-off was also achieved in these non-doped OLEDs. The non-doped OLED based on *pp*CTPI exhibited a maximum L, η_c, η_p and EQE of up to 31 070 cd m^{-2}, 18.46 cd A^{-1}, 16.32 lm W^{-1} and 7.16%, respectively. Notably, the device showed excellent efficiency stability, as evidenced by the very small efficiency roll-off of 4.0% at 1000 cd m^{-2}.

Conclusions

In order to enhance the PLQYs of HLCT-based compounds in aggregates and develop a feasible molecular design strategy for high-efficiency OLED emitters by incorporating TPE units and cyano groups at the C2 and N1 positions with different patterns, six fluorescent PI derivatives were prepared. The systematic photophysical analysis in various formations showed that the six compounds exhibited AIE characteristics with high PLQYs in aggregates and had a tunable excited-state distribution of LE and CT components in HLCT states. Combining the photophysical and electrochemical measurements and theoretical calculations, the impacts of the molecular conjugation patterns on the LE/CT distribution, luminous efficiency, and exciton conversion channel were revealed, based on which the contributions of the crossed axes (long axis and short axis) with a vertical conformation was proposed. The performances of non-doped OLEDs based on these PI derivatives proved our hypothesis. Amongst these compounds, *pp*CTPI exhibited the best EL performance with a maximum L, η_c and η_p of up to 31 070 cd m^{-2}, 18.46 cd A^{-1}, 16.32 lm W^{-1} and a maximum EQE of 7.16% with a roll-off of 4.0% at 1000 cd m^{-2} luminance. These results demonstrated that the strategy of reasonably superposing the AIE unit onto HLCT emitters by constructing a conformation of vertical cross axes is practically feasible in materials design.

Conflicts of interest

There are no conflicts to declare.

Acknowledgements

This work is financially supported by the National Natural Science Foundation of China (21788102, 51673118 and 51603127), the Guangdong Natural Science Funds for Distinguished Young Scholars (2014A030306035), the Science & Technology Program of Guangzhou (201804010218, 201804020027, 201704030069), the Innovation and Technology Commission of Hong Kong (ITC-CNERC14SC01), and the Fundamental Research Funds for the Central Universities (2017JQ013).

Notes and references

1 (*a*) M. A. Baldo, M. E. Thompson and S. R. Forrest, *Nature*, 2000, **403**, 750; (*b*) A. C. Grimsdale, K. L. Chan, R. E. Martin, P. G. Jokisz and A. B. Holmes, *Chem. Rev.*, 2009, **109**, 897.

2 M. A. Baldo, D. F. O'Brien, M. E. Thompson and S. R. Forrest, *Phys. Rev. B: Condens. Matter Mater. Phys.*, 1999, **60**, 14422.

3 (*a*) H. Uoyama, K. Goushi, K. Shizu, H. Nakamura and C. Adachi, *Nature*, 2012, **492**, 234; (*b*) Y. Geng, A. D'Aleo, K. Inada, L.-S. Cui, J. U. Kim, H. Nakanotani and C. Adachi, *Angew. Chem., Int. Ed.*, 2017, **56**, 16536; (*c*) J. Guo, X.-L. Li, H. Nie, W. Luo, S. Gan, S. Hu, R. Hu, A. Qin, Z. Zhao, S.-J. Su and B. Z. Tang, *Adv. Funct. Mater.*, 2017, **27**, 1606458; (*d*) D. Zhang, X. Song, M. Cai, H. Kaji and L. Duan, *Adv. Mater.*, 2018, **30**, 1705406; (*e*) X. Chen, Z. Yang, Z. Xie, J. Zhao, Z. Yang, Y. Zhang, M. P. Aldred and Z. Chi, *Mater. Chem. Front.*, 2018, **2**, 1017.

4 (*a*) D. Yang, P. Duan and M. Liu, *Angew. Chem., Int. Ed.*, 2018, **57**, 9357; (*b*) J. Han, Y. Jiang, A. Obolda, P. Duan, F. Li and M. Liu, *J. Phys. Chem. Lett.*, 2017, **8**, 5865; (*c*) P. Duan, N. Yanai, Y. Kurashige and N. Kimizuka, *Angew. Chem., Int. Ed.*, 2015, **54**, 7544; (*d*) X. Tang, Q. Bai, T. Shan, J. Li, Y. Gao, F. Liu, H. Liu, Q. Peng, B. Yang, F. Li and P. Lu, *Adv. Funct. Mater.*, 2018, **28**, 1705813.

5 (*a*) W. Li, D. Liu, F. Shen, D. Ma, Z. Wang, T. Feng, Y. Xu, B. Yang and Y. Ma, *Adv. Funct. Mater.*, 2012, **22**, 2797; (*b*) R. K. Konidena, K. R. Justin Thomas, D. Kumar Dubey, S. Sahoo and J. H. Jou, *Chem. Commun.*, 2017, **53**, 11802; (*c*) Y. Gao, S. Zhang, Y. Pan, L. Yao, H. Liu, Y. Guo, Q. Gu, B. Yang and Y. Ma, *Phys. Chem. Chem. Phys.*, 2016, **18**, 24176; (*d*) C. Wang, X.-L. Li, Y. Gao, L. Wang, S. Zhang, L. Zhao, P. Lu, B. Yang, S.-J. Su and Y. Ma, *Adv. Opt. Mater.*, 2017, **5**, 1700441.

6 (*a*) B. Li, G. Tang, L. Zhou, D. Wu, J. Lan, L. Zhou, Z. Lu and J. You, *Adv. Funct. Mater.*, 2017, **27**, 1605245; (*b*) W. Z. Yuan, X. Bin, G. Chen, Z. He, J. Liu, H. Ma, Q. Peng, B. Wei, Y. Gong, Y. Lu, G. He and Y. Zhang, *Adv. Opt. Mater.*, 2017, **5**, 1700466; (*c*) S. Zhang, W. Li, L. Yao, Y. Pan, F. Shen, R. Xiao, B. Yang and Y. Ma, *Chem. Commun.*, 2013, **49**, 11302; (*d*) Y. Pan, W. Li, S. Zhang, L. Yao, C. Gu, H. Xu, B. Yang and Y. Ma, *Adv. Opt. Mater.*, 2014, **2**, 510.

7 (*a*) Y. Hong, J. W. Y. Lam and B. Z. Tang, *Chem. Soc. Rev.*, 2011, **40**, 5361; (*b*) J. Mei, N. Leung, R. Kwok, J. W. Y. Lam and B. Z. Tang, *Chem. Rev.*, 2015, **115**, 11718; (*c*) Z. Zhao, B. He and B. Z. Tang, *Chem. Sci.*, 2015, **6**, 5347; (*d*) L. Pan, Y. Cai., H. Wu, F. Zhou, A. Qin, Z. Wang and B. Z. Tang, *Mater. Chem. Front.*, 2018, **2**, 1310.

8 (*a*) J. D. Luo, Z. L. Xie, J. W. Y. Lam, L. Cheng, H. Y. Chen, C. F. Qiu, H. S. Kwok, X. W. Zhan, Y. Q. Liu, D. B. Zhu and B. Z. Tang, *Chem. Commun.*, 2001, 1740; (*b*) H. Nie, K. Hu, Y. Cai, Q. Peng, Z. Zhao, R. Hu, S.-J. Su, J. Chen, A. Qin and B. Z. Tang, *Mater. Chem. Front.*, 2017, **1**, 1125; (*c*) Q. Li and Z. Li, *Adv. Sci.*, 2017, **4**, 1600484.

9 (*a*) Z. Zhao, J. W. Y. Lam and B. Z. Tang, *J. Mater. Chem.*, 2012, **22**, 23726; (*b*) J. Yang, J. Huang, Q. Q. Li and Z. Li, *J. Mater. Chem. C*, 2016, **4**, 2663; (*c*) F. Song, Z. Xu, Q. Zhang, Z. Zhao, H. Zhang, W. Zhao, Z. Qiu, C. Qi, H. Zhang, H. H. Y. Sung, I. D. Williams, J. W. Y. Lam, Z. Zhao, A. Qin, D. Ma and B. Z. Tang, *Adv. Funct. Mater.*, 2018, **28**, 1800051; (*d*) J. Yang, L. Li, Y. Yu, Z. Ren, Q. Peng, S. Ye, Q. Li and Z. Li, *Mater. Chem. Front.*, 2017, **1**, 91–99; (*e*) Z. Li, *Sci. China: Chem.*, 2017, **60**, 1107–1108.

10 (*a*) M. Y. Bian, Z. F. Zhao, Y. Li, Q. Li, Z. J. Chen, D. D. Zhang, S. F. Wang, Z. Q. Bian, Z. W. Liu, L. Duan and L. X. Xiao, *J. Mater. Chem. C*, 2018, **6**, 745; (*b*) T. X. Liu, L. P. Zhu, C. Zhong, G. H. Xie, S. L. Gong, J. F. Fang, D. G. Ma and C. L. Yang, *Adv. Funct. Mater.*, 2017, **27**, 1606384; (*c*) T. C. Yu, L. L. Liu, Z. Q. Xie and Y. G. Ma, *Sci. China: Chem.*, 2015, **58**, 907.

11 (*a*) Z. Wang, X. Li, K. Xue, H. Li, X. Zhang, Y. Liu, Z. Yu, P. Lu and P. Chen, *J. Mater. Chem. C*, 2016, **4**, 1886; (*b*) Z. Wang, Y. Feng, S. Zhang, Y. Gao, Z. Gao, Y. Chen, X. Zhang, P. Lu, B. Yang, P. Chen, Y. Ma and S. Liu, *Phys. Chem. Chem. Phys.*, 2014, **16**, 20772; (*c*) S. Zhang, L. Yao, Q. Peng, W. Li, Y. Pan, R. Xiao, Y. Gao, C. Gu, Z. Wang, P. Lu, F. Li, S. Su, B. Yang and Y. Ma, *Adv. Funct. Mater.*, 2015, **25**, 1755.

12 (*a*) Z. Gao, K. Wang, F. Liu, C. Feng, X. He, J. Li, B. Yang, B. Zou and P. Lu, *Chem. – Eur. J.*, 2017, **23**, 773; (*b*) B. Xu, J. He, Y. Mu, Q. Zhu, S. Wu, Y. Wang, Y. Zhang, C. Jin, C. Lo, Z. Chi, A. Lien, S. Liu and J. Xu, *Chem. Sci.*, 2015, **6**, 3236.

13 Y. Yuan, J. Chen, F. Lu, Q. Tong, Q. Yang, H. Mo, T. Ng, F. Wong, Z. Guo, J. Ye, Z. Chen, X. Zhang and C. Lee, *Chem. Mater.*, 2013, **25**, 4957.

14 J. Yang, Q. X. Guo, J. Q. Wang, Z. C. Ren, J. X. Chen, Q. Peng, D. G. Ma and Z. Li, *Adv. Opt. Mater.*, 2018, **6**, 1800342.

15 (*a*) B. Chen, H. Zhang, W. Luo, H. Nie, R. Hu, A. Qin, Z. Zhao and B. Z. Tang, *J. Mater. Chem. C*, 2017, **5**, 960–968; (*b*) Y. Cai, C. Shi, H. Zhang, B. Chen, K. Samedov, M. Chen, Z. Wang, Z. Zhao, X. Gu, D. Ma, A. Qin and B. Z. Tang, *J. Mater. Chem. C*, 2018, **6**, 6534; (*c*) Y. Cai, C. Gui, K. Samedov, H. F. Su, X. G. Gu, S. W. Li, W. W. Luo, H. H. Y. Sung, J. W. Y. Lam, R. T. K. Kwok, I. D. Williams, A. J. Qin and B. Z. Tang, *Chem. Sci.*, 2017, **8**, 7593.

16 (*a*) T. Nakagawa, S. Y. Ku, K. T. Wong and C. Adachi, *Chem. Commun.*, 2012, **48**, 9580; (*b*) J. Guo, X. L. Li, H. Nie, W. W. Luo, R. R. Hu, A. J. Qin, Z. J. Zhao, S. J. Su and B. Z. Tang, *Chem. Mater.*, 2017, **29**, 3623.

17 S. Tang, W. J. Li, F. Z. Shen, D. D. Liu, B. Yang and Y. G. Ma, *J. Mater. Chem.*, 2012, **22**, 4401.

18 (*a*) D. Hu, F. Shen, H. Liu, P. Lu, Y. Lv, D. Liu and Y. Ma, *Chem. Commun.*, 2012, **48**, 3015; (*b*) H. Liu, P. Chen, D. Hu, X. Tang, Y. Pan, H. Zhang, W. Zhang, X. Han, Q. Bai, P. Lu and Y. Ma, *Chem. – Eur. J.*, 2014, **20**, 2149.

19 (*a*) S. K. Kim, B. Yang, Y. I. Park, Y. G. Ma, J. Y. Lee, H. J. Kim and J. Park, *Org. Electron.*, 2009, **10**, 822; (*b*) B. Yang, S. K. Kim, H. Xu, Y. I. Park, H. Y. Zhang, C. Gu, F. Z. Shen, C. L. Wang, D. D. Liu, X. D. Liu, M. Hanif, S. Tang, W. J. Li, F. Li, J. C. Shen, J. W. Park and Y. Ma, *ChemPhysChem*, 2008, **9**, 2601.

20 Z. R. Grabowski, K. Rotkiewicz and W. Rettig, *Chem. Rev.*, 2003, **103**, 3899.

21 J. R. Sheats, H. Antoniadis, M. Hueschen, W. Leonard, J. Miller, R. Moon, D. Roitman and A. Stocking, *Science*, 1996, **273**, 884.

22 (*a*) M. Segal, M. Singh, K. Rivoir, S. Difley, T. V. Voorhis and M. A. Baldo, *Nat. Mater.*, 2007, **6**, 374; (*b*) S. Difley, D. Beljonne and T. V. Voorhis, *J. Am. Chem. Soc.*, 2008, **130**, 3420.

23 Z. Wang, P. Lu, S. Chen, Z. Gao, F. Shen, W. Zhang, Y. Xu, H. Kwok and Y. Ma, *J. Mater. Chem.*, 2011, **21**, 5451.

24 D. Dang, Z. Wang, K. Liu, Y. Liu, H. Sung, I. Willians, R. Kwok, J. W. Y. Lam, S.-J. Su and B. Z. Tang, *Adv. Electron. Mater.*, 2018, **4**, 1800354.

